UVRAG is required for virus entry through combinatorial interaction with the class C-Vps complex and SNAREs

Sara Dolatshahi Pirooz[a], Shanshan He[a], Tian Zhang[a], Xiaowei Zhang[a], Zhen Zhao[a], Soohwan Oh[a], Douglas O'Connell[a], Payam Khalilzadeh[a], Samad Amini-Bavil-Olyaee[a], Michael Farzan[b], and Chengyu Liang[a,1]

[a]Department of Molecular Microbiology and Immunology, Keck School of Medicine, University of Southern California, Los Angeles, CA 90033; and [b]Department of Infectious Diseases, The Scripps Research Institute, Jupiter, FL 33458

Edited by Peter Palese, Icahn School of Medicine at Mount Sinai, New York, NY, and approved January 15, 2014 (received for review November 4, 2013)

Enveloped viruses exploit the endomembrane system to enter host cells. Through a cascade of membrane-trafficking events, virus-bearing vesicles fuse with acidic endosomes and/or lysosomes mediated by SNAREs triggering viral fusion. However, the molecular mechanisms underlying this process remain elusive. Here, we found that UV-radiation resistance-associated gene (UVRAG), an autophagic tumor suppressor, is required for the entry of the prototypic negative-strand RNA virus, including influenza A virus and vesicular stomatitis virus, by a mechanism independent of IFN and autophagy. UVRAG mediates viral endocytic transport and membrane penetration through interactions with the class C vacuolar protein sorting (C-Vps) tethering complex and endosomal glutamine-containing SNAREs [syntaxin 7 (STX7), STX8, and vesicle transport through t-SNARE homolog 1B (Vti1b)], leading to the assembly of a fusogenic *trans*-SNARE complex involving vesicle-associated membrane protein (VAMP8), but not VAMP7. Indeed, UVRAG stimulates VAMP8 translocation to virus-bearing endosomes. Inhibition of VAMP8, but not VAMP7, significantly reduces viral entry. Our data indicate that UVRAG, in concert with C-Vps, regulates viral entry by assembling a specific fusogenic SNARE complex. Thus, UVRAG governs downstream viral entry, highlighting an important pathway capable of potential antiviral therapeutics.

endocytic trafficking | influenza virus | VSV

Viruses are obligate intracellular parasites that must enter host cells for replication. Although some viruses penetrate cells directly through the plasma membrane, most take advantage of existing portals of entry evolved for nutrient uptake and receptor signaling while moving within the endosomal apparatus of the cell to reach the site for replication (1). Among the best-studied examples is vesicular stomatitis virus (VSV), a prototype of the Rhabdoviridae, which has long been used as a model to understand viral entry mechanisms and host endosome biology (1). Although it is established that transport to the acidic endosome is required for release of VSV and other negative-strand RNA viruses, such as influenza A virus (IAV) (1, 2), the molecular machinery that ferries these viruses through the endomembrane remains poorly understood. Moreover, the ride is not free for the virus because the lysosome station on the endocytic pathway is a potentially hazardous environment that degrades viral components and reports infection. How the virus traffics within, and eventually escapes from, specific endosomal organelles before lysosome degradation is another important question in virus entry.

Evidence shows that endocytic transport is not a random priming event hitchhiked by the virus, but an important strategy the virus exploits to route itself to a specific compartment for fusion and genome release (1). This process is achieved by SNARE-regulated sequential fusion between virion-containing vesicles and intracellular organelles, including early endosomes, late endosomes (LEs), and lysosomes (3). Fusogenic *trans*-SNARE complexes are assembled to form a four-helix bundle consisting of glutamine (Q) a-, Qb-, and Qc-SNAREs embedded in one membrane and arginine (R)-SNAREs embedded in the other (3). Specifically, syntaxin 7 (STX7; Qa), Vti1b (Qb), and STX8 (Qc) on the LE, when paired with VAMP7 (R), mediate the LE fusion with the lysosome, but when paired with VAMP8 (R), regulate homotypic fusion of the LEs (4). The upstream process regulating LE-associated SNARE pairing relies on the class C vacuolar protein sorting (Vps) complex (hereafter referred to as C-Vps), composed of Vps11, Vps16, Vps18, and Vps33 as core subunits (5, 6). A recent study indicated that C-Vps interaction with endosomal Q-SNAREs allows the assembly of fusogenic *trans*-SNAREs leading to vesicle fusion (5). The C-Vps complex was also found to mediate the entry of Ebola virus (7), but the mechanism of action remains unknown.

Our previous studies identified UV-radiation resistance-associated gene (*UVRAG*) as a positive regulator of the C-Vps complex, which interacts with C-Vps through its C2 domain (8). Deletion of UVRAG causes a C-Vps phenotype, and it blocks endosomal maturation and down-regulation of cell surface receptors targeted for lysosomal degradation (8). Furthermore, UVRAG has a unique activity in autophagy, where it forms a complex with Beclin1 and activates Beclin1-associated class III PI3K activity (9, 10). Our recent work further established that UVRAG patrols chromosomal stability and endoplasmic reticulum-Golgi homeostasis independent of autophagy (11, 12). Despite these findings, the functionality of UVRAG in a cell's response to virus infection has not yet been examined. In this study, we demonstrate that

Significance

Negative-strand RNA viruses are highly pathogenic and cause many severe diseases in humans and animals. These viruses generally use existing cellular pathways to enter cells, which involves intensive interaction with the endomembrane network, offering the endocytic pathway as an attractive scheme for therapeutic intervention. Molecular mechanisms governing virus entry remain incompletely understood. We found that UV-radiation resistance-associated gene, well known for regulating autophagy and intracellular trafficking, is a critical factor for virus entry through combinatorial interactions with a tether and endosomal SNAREs. Understanding the mechanism that allows the virus to interact with late endocytic organelles could identify the specific set of proteins that have a role in virus entry, which will help us to design specific therapeutic agents against endocytic virus entries.

Author contributions: S.D.P. and C.L. designed research; S.D.P., S.H., T.Z., S.O., P.K., and C.L. performed research; Z.Z., S.O., and S.A.-B.-O. contributed new reagents/analytic tools; S.D.P., S.H., T.Z., X.Z., Z.Z., D.O., M.F., and C.L. analyzed data; and S.D.P., D.O., and C.L. wrote the paper.

The authors declare no conflict of interest.

This article is a PNAS Direct Submission.

[1]To whom correspondence should be addressed. E-mail: chengyu.liang@usc.edu.

This article contains supporting information online at www.pnas.org/lookup/suppl/doi:10.1073/pnas.1320629111/-/DCSupplemental.

UVRAG has a distinct role in mediating virus entry, working in concert with C-Vps and the endosomal SNAREs during late endocytic membrane fusion. We have also identified specific SNAREs and their interactions that are reprogrammed by the virus to assist in their entry and infection.

Results

VSV Replication Is Suppressed in UVRAG-Deficient Cells. To investigate whether UVRAG is involved in the cell's response to RNA virus infection, we depleted endogenous UVRAG from HeLa cells by shRNA and infected them with recombinant VSV expressing GFP (rVSV-GFP) as a reporter. Knockdown of UVRAG resulted in a substantial reduction in VSV replication, compared with control shRNA-treated cells (Fig. 1 *A*, *B*, and *D*). Both the number of cells expressing GFP (Fig. 1*B*) and the abundance of viral RNA encoding glycoprotein G (Fig. 1*C*) were markedly reduced in UVRAG-depleted cells. To verify this, we further assessed VSV infectivity in mouse ES cells with allelic loss of *UVRAG* gene ($UVRAG^{+/-}$) (Fig. 1 *E*–*G*). Compared with the WT control ($UVRAG^{+/+}$), $UVRAG^{+/-}$ cells were significantly less susceptible after infection with different doses [multiplicity of infection (MOI)] of VSV, with the virus titers dropping precipitously (Fig. 1*F*). The replication restriction in $UVRAG^{+/-}$ cells was reverted when WT UVRAG was reintroduced, suggesting that this is not an off-target, but a UVRAG-specific, effect (Fig. S1 *A* and *B*). Consistent with the resistance to viral infection in UVRAG-deficient cells, ectopic expression of UVRAG in UVRAG-deficient HCT116 cells markedly increased infection compared with control, as shown by the proportionality in GFP signals at varying MOIs (Fig. S1 *C* and *D*). Taken together, these data indicate that UVRAG is required for efficient VSV infection.

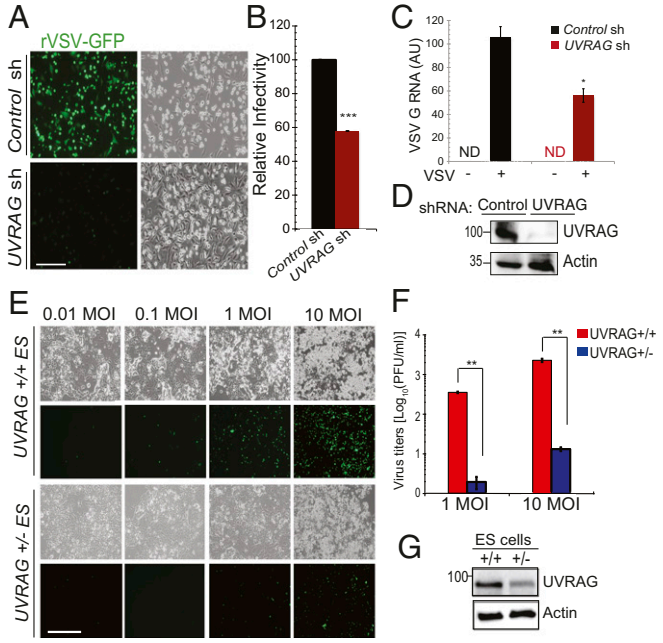

Fig. 1. UVRAG is required for VSV replication. (*A* and *B*) Impaired VSV replication in UVRAG knockdown cells. (*A*) HeLa cells were pretreated with control- or UVRAG-specific shRNA for 72 h and then infected (MOI of 10) with rVSV-GFP and processed for immunofluorescence microscopy. sh, short hairpin. (Scale bar, 50 μm.) (*B*) Viral infectivity is expressed as mean GFP fluorescence relative to control cells, as determined by flow cytometry. Values represent mean ± SD ($n = 3$ independent experiments). ***$P < 0.001$. (*C*) Quantitative RT-PCR analysis of RNA encoding the VSV G protein in control sh-transduced and UVRAG sh-transduced HeLa cells mock-infected or infected for 8 h with rVSV-GFP. ND, not detectable. *$P < 0.05$. AU, artificial unit. (*D*) Western blot shows the expression of endogenous UVRAG, and actin serves as a loading control. (*E*–*G*) Fluorescence microscopy analysis of $UVRAG^{+/+}$ and $UVRAG^{+/-}$ ES cells infected for 8 h with rVSV-GFP at the indicated MOIs. Viral infectivity in *E* was determined by plaque assay (*F*), and the Western blot shows the levels of UVRAG in these cells (*G*). Data represent mean ± SD ($n = 4$). **$P < 0.01$. (Scale bar, 50 μm.)

Effect of UVRAG on Viral Infection Is Not IFN-Dependent. How does UVRAG promote viral infection? A simple interpretation would be an altered type I IFN response, the first line of defense against virus infection (13). To test this, we compared the levels of type I IFN production between control and UVRAG knockdown cells after stimulation of polyinosinic:polycytidylic acid [poly(I:C)], a potent inducer of type I IFN. We found that untreated cells had marginal expression of *Ifnα* and *Ifnβ* mRNA, and that treatment with poly(I:C) stimulated similarly high *Ifnα* and *Ifnβ* mRNA expression in WT and UVRAG knockdown cells (Fig. S2 *A* and *B*). To verify this, we collected culture medium from control and UVRAG knockdown cells after poly(I:C) treatment and examined its protection of naive HeLa cells against VSV infection (Fig. S2*C*). Although the virus titers were drastically reduced in the poly(I:C)-treated cultures by >90%, no discernible difference was observed between control and UVRAG knockdown cultures (Fig. S2 *D* and *E*). These results indicate that UVRAG does not affect overall type I IFN production and UVRAG-induced VSV infection is not due to an altered IFN response.

Autophagy-Independent Role of UVRAG in Viral Infection. We next assessed whether the virus-resistant phenotype of UVRAG-deficient cells was due to inhibition of autophagy. This seemed unlikely, because repression of autophagy was found to increase VSV replication in cultured cells (14, 15). Consistent with this view, we detected a robust increase of viral GFP in autophagy-deficient cells, including $Atg5^{-/-}$, $Atg7^{-/-}$, and $Atg16^{+/-}$ immortalized mouse embryonic fibroblasts after infection with increasing doses of VSV (Fig. S3 *A*–*C*), suggesting that the autophagy pathway is largely antiviral. Nonetheless, to rule out the possibility of autophagy participation, we examined the effect of UVRAG knockdown on VSV infection in the autophagy-deficient Atg5 KO cells. We found that whereas loss of Atg5 increased viral replication as noted before (14, 15), depletion of UVRAG significantly reduced virus titers (50- to 100-fold) regardless of Atg5 activity (Fig. S3 *D*–*F*). These data indicate that UVRAG is necessary for viral infection through a nonautophagic mechanism.

UVRAG Is Required for Efficient Virus Entry. To determine which step in the replication cycle was affected by UVRAG, we forced fusion of the viral envelope with the plasma membrane by adding medium with a low pH (pH = 5.0) to cells with bound virus. By doing this, the normal route of entry of VSV via endocytic transport was bypassed, leading to the direct release of viral genomes into the cytosol for replication (16). Under this condition, VSV replication was insensitive to UVRAG and no discernible difference was detected between control and UVRAG knockdown cells (Fig. S4*A*). Notably, the low-pH–induced membrane fusion was sufficient because the virus exhibited resistance to bafilomycin, which blocks the acidification of endosomes, and therefore of mature VSV entry (Fig. S4*A*). We also observed that UVRAG knockdown did not affect the numbers of virions being internalized into cells at 5 min and 15 min after infection, suggesting no defect in the early virus uptake (Fig. S4*B*). These data suggest that VSV replication was impaired at an early stage of infection in cells lacking UVRAG, somewhere between viral uptake and the release of viral nucleocapsid.

We next investigated whether UVRAG regulated the endocytic virus entry. To this end, we conducted a single-cycle entry assay in UVRAG-depleted cells. This assay uses defective pseudo-retroviruses carrying different viral envelopes as entry factors and GFP as an indicator (17, 18). As such, infection of these pseudoviruses differs only in the entry step mediated by their respective envelope

MICROBIOLOGY

proteins (18). We found that down-regulation of UVRAG considerably inhibited VSV-glycoprotein G (VSV-G)–pseudotyped virus infection (Fig. 2*A*), whereas no inhibition was observed with Lassa virus (LASV) and lymphocytic choriomeningitis virus (LCMV), which use a different pathway to enter cells (19, 20). There was a fourfold increase in VSV-G–mediated pseudovirus infection in HCT116 and HeLa cells stably expressing UVRAG, whereas LASV infection remained unaffected by UVRAG (Fig. S4 *C* and *D*). To determine whether the entry block in UVRAG-deficient cells was unique for VSV, we infected cells with the pseudoviruses carrying the entry proteins of IAV PR8 (H1N1), Udorn (H3N1), and Thai (H5N1) (Fig. 2 *A* and *B*). Similar to VSV, none of the three IAVs replicated efficiently in UVRAG-depleted cells, and their infectivity was 20% of that observed in WT cells (Fig. 2 *A* and *B*). These results indicate that UVRAG is essential for the entry of VSV, IAV, and likely other endocytic RNA viruses.

UVRAG Promotes Endocytic Transport of Virions. To assess the mechanism of action of UVRAG in virus entry, we used a viral fusion assay that tracks the real-time entry of virions in living cells (2, 21). We labeled VSV with the self-quenching dye DiI (Molecular Probes, Invitrogen), which is incorporated into the virion envelopes without affecting their infectivity (2, 21). Upon binding onto the cell surface at 4 °C, DiI-labeled VSV was not fluorescent (Fig. S4*E*; $t = 0$). When cells were incubated at 37 °C to trigger viral entry, the endocytic transport of DiI-labeled VSV and its exposure to acidic endosomes were visualized as red particles due to acid-induced dye dequenching and fusion (Fig. S4*E*; t =30). Knockdown of UVRAG resulted in a substantial reduction in intracellular DiI-labeled VSV (Fig. S4 *E–G*). The signals were specific because they were abolished when treated with bafilomycin A1, which neutralizes endosomal pH (Fig. S4*G*). We also examined the intracellular distribution of the Matrix (M) protein of native VSV to the cytoplasm as a marker for membrane fusion (7). Control cells had diffused distribution of M protein (Fig. S4*H*). By contrast, only punctate, perinuclear staining of M protein was detected in infected cells with *UVRAG* knockdown, which was further blocked by bafilomycin A1 or nocodazole (Fig. S4 *H* and *I*). These data suggest that viral fusion is inhibited upon UVRAG deficiency.

To examine whether UVRAG routes virions to acidic endosomes for membrane fusion, we examined the distribution of endocytosed VSV (as indicated by the staining of VSV-G) within 1 h after infection relative to lysobisphosphatidic acid (LBPA), which accounts for the vast majority of LE membranes (22) and promotes viral fusion (23). In agreement with reports that productive VSV fusion takes place in LEs (2), we found that most VSV-G colocalized with the juxtanuclear LBPA$^+$ LEs in control cells at 45 min after infection. By contrast, there was a significant reduction in the costaining of VSV-G and LBPA upon UVRAG depletion (Fig. 2 *C* and *D*). A similar reduction was also observed when cells were treated with nocodazole, which depolymerizes microtubules interrupting endosomal transport (Fig. 2 *C* and *D*). Of note, the LBPA-containing membranes remained unchanged upon UVRAG knockdown, and equivalent numbers of virions were endocytosed into cells (Fig. 2*C* and Fig. S4*B*). To further verify that this is entry-related, we infected cells with the VSV-G–coated pseudovirus. Again, knockdown of UVRAG and/or treatment of cells with nocodazole drastically inhibited the acquisition of LBPA$^+$ membrane to the pseudovirion-containing vesicles (Fig. S4*J*). Together, these results indicate that UVRAG is required for the late endocytic transport of the virus, leading to efficient membrane fusion and productive penetration.

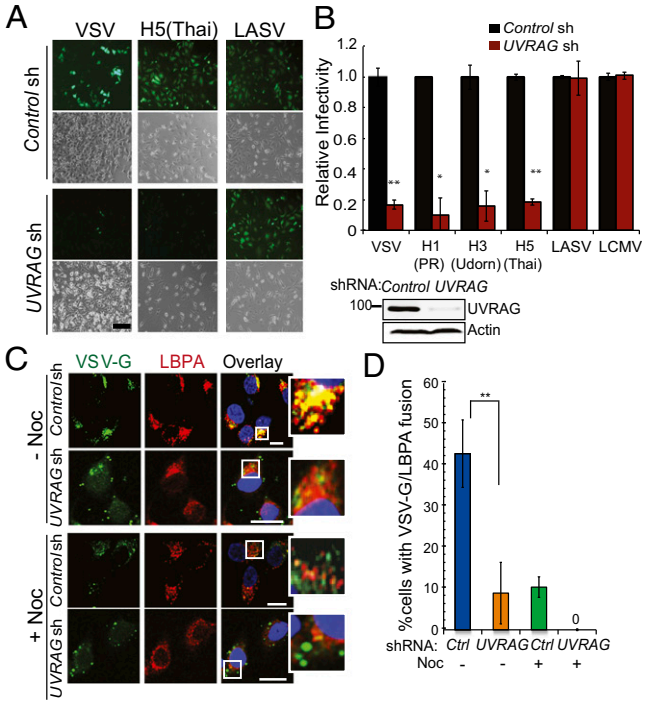

Fig. 2. UVRAG is required for efficient virus entry. (*A* and *B*) UVRAG knockdown impairs virus entry of VSV and IAV. HeLa cells were transfected with control- or UVRAG-specific shRNA and then infected with MLV-GFP pseudotyped with the indicated envelope protein [VSV, IAV H1N1 (PR8), IAV H3N1 (Udom), IAV H5N1 (Thai), LASV, or LCMV]. (*A*) Representative images of viral infection (green) are shown. (Scale bar, 50 μm.) (*B*) Viral entry is expressed as mean GFP fluorescence relative to control cells, as determined by flow cytometry. Values represent mean ± SD (n = 5 independent experiments). (*Lower Right*) Western blot shows the expression of UVRAG in cells. *$P < 0.05$; **$P < 0.01$. (*C* and *D*) UVRAG is required for viral access to LE compartments. HeLa cells were transfected with control- or UVRAG-specific shRNA, preincubated with 10 μM nocadazole (+Noc) or without (−Noc) for 2 h, and then infected with VSV (MOI of 0.5) for 45 min. Infected cells were fixed and immunostained with antibody against VSV-G (green) and LBPA (red). (*C*) Representative images from three independent experiments are shown. Note that colocalization between VSV-G and LBPA was observed in control cells and highlighted (*Insets*) but was inhibited by UVRAG knockdown or by Noc treatment. (Scale bar, 20 μm.) (*D*) Percentage of infected cells with VSV-G staining colocalized with LBPA was quantified. Data represent mean ± SD (n = 100) from three independent experiments. **$P < 0.01$. Ctrl, control.

Domains of UVRAG Required for Virus Entry. Next, we performed a structure/function analysis to map the domain of UVRAG responsible for virus entry. We expressed Flag-tagged WT and mutant UVRAG proteins at equivalent levels in HCT116 cells and assessed the ability of these mutants to promote the entry of pseudoviruses bearing the entry proteins of VSV, IAV, and LASV.

UVRAG contains an N-terminal C2 domain (residues 42–147), followed by a central coiled-coil domain (CCD; residues 200–269) and a C-terminal region (residues 270–699) (Fig. S5*A*). We found that unlike WT UVRAG, which promotes the entry of VSV and IAV, but not that of LASV, UVRAG lacking the C2 (ΔC2) or coiled-coil domain (CCD) (ΔCCD) domain both failed to promote cells' susceptibility to VSV and IAV infection (Fig. 3 *A* and *B*). Moreover, expression of the ΔC2 mutant had a dominant-negative phenotype, drastically inhibiting the entry of the viruses by more than 90% compared with the vector (Fig. 3 *A* and *B*). We also detected much lower abundance of VSV G proteins in ΔCCD and ΔC2 cells after native VSV infection (Fig. S5*B*). Consistently, intracellular transport of VSV to LBPA$^+$ vesicles was markedly reduced to 50% and 5% of WT levels by the expression of ΔCCD and ΔC2, respectively (Fig. S5 C and *D*). These results indicate that both the C2 and CCD domains are required for UVRAG to promote virus entry.

C-Vps, but Not Beclin1, Is Required for UVRAG-Mediated Virus Entry. Our previous studies showed that the C2 of UVRAG associates with C-Vps to enhance endocytic protein degradation, whereas the CCD binds Beclin1 and activates Beclin1-mediated autophagy (8, 9). We next determined the importance of C-Vps and Beclin1 in UVRAG-mediated viral infection. As observed with UVRAG knockdown, treatment of cells with Vps16- or Vps18-siRNA, but not with scrambled siRNA, significantly suppressed VSV replication at different MOIs (Fig. S6 *A* and *B*). To confirm the significance of UVRAG–C-Vps interaction in viral infection, we depleted Vps18 from cells expressing WT or mutant UVRAG and found that removal of Vps18 diminished the capability of UVRAG to promote VSV infection (Fig. S6 *C–E*). Our results demonstrate that UVRAG and its interaction with C-Vps are required for VSV infection.

Unlike depletion of C-Vps, knockdown of Beclin1 showed minimal effect on VSV replication (Fig. S6*F*). Likewise, no reduction in viral infection was observed in WT or mutant UVRAG-expressing cells by inhibition of Beclin1 (Fig. S6 *G–I*). Although UVRAG ΔCCD inhibited viral entry, Beclin1 is clearly not required in this activity; other factor(s) may be involved with respect to CCD function. Collectively, these results demonstrate that UVRAG interactions with C-Vps, but not Beclin1, are important for efficient viral infection.

UVRAG Interacts with SNAREs. One essential role of C-Vps in endosomal transport is to facilitate assembly of the fusogenic SNARE complex, including STX7, Vti1b, and STX8, pairing with VAMP8 or VAMP7 in the homotypic or heterotypic fusion of LEs, respectively (4, 24). We asked whether UVRAG, like its interactor C-Vps, also binds SNAREs on LEs/lysosomes, whereby much acid-induced virus fusion takes place (25). Our immunoprecipitation analyses demonstrated that both endogenous and Flag-tagged UVRAG efficiently coprecipitated with endogenous Q-SNAREs (i.e., STX7, Vti1b, STX8) (Fig. 4*A* and Fig. S7*A*). No discernible interaction was detected with VAMP7 and VAMP8 or with STX6, which is the *trans*-Golgi–related SNARE, suggesting a compartment-specific Q-SNARE interaction of UVRAG (Fig. 4*A*). Moreover, the CCD is sufficient and necessary for the interaction of UVRAG with Q-SNAREs (Fig. S7 *A* and *B*). Notably, the ΔC2 mutant of UVRAG, defective in C-Vps binding (8), preserved efficient interaction with Q-SNAREs (Fig. S7*A*), suggesting that UVRAG association with Q-SNAREs is not dependent on its interaction with C-Vps. Because the CCD of UVRAG directly binds Beclin1 (9), we asked whether Beclin1 is involved in the UVRAG–SNARE interactions. As shown in Fig. S7*C*, depletion of Beclin1 did not alter the binding efficiency of UVRAG with Q-SNAREs. These results indicate that UVRAG forms a complex with endosomal Q-SNAREs through its CCD in a Beclin1-independent manner (Fig. S7*G*).

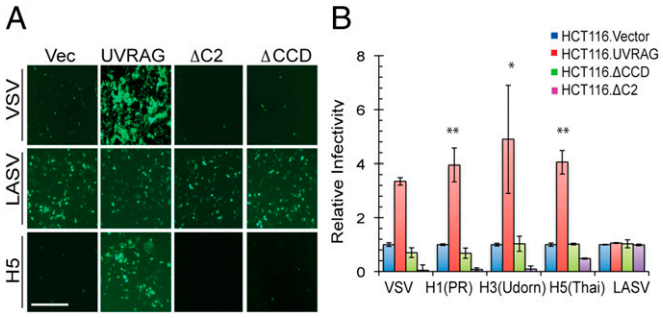

Fig. 3. Domains of UVRAG required for virus entry. HCT116 cells stably expressing vector and Flag-tagged UVRAG or its ΔC2 or ΔCCD mutant were infected with MLV-GFP virus pseudotyped with the indicated entry protein for 48 h. Pseudovirus infectivity (green) was visualized by fluorescence microscopy (*A*), and viral entry is expressed as mean GFP fluorescence relative to the vector (Vec) cells, as examined by flow cytometry (*B*). Data represent mean ± SD ($n = 4$ independent experiments). *$P < 0.05$; **$P < 0.01$. (Scale bar, 50 μm.)

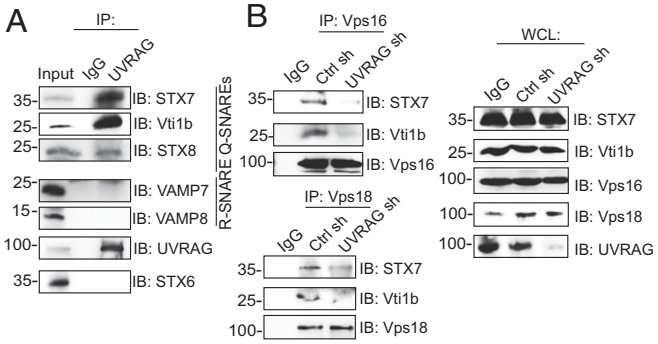

Fig. 4. UVRAG functions together with C-Vps and SNAREs. (*A*) Endogenous interaction of UVRAG with endosomal SNAREs. Whole-cell lysates (WCLs) of 293T cells were used for immunoprecipitation (IP) with control serum (IgG) or anti-UVRAG, followed by immunoblotting (IB) with the indicated antibodies. Ten percent of the WCLs were used as input. (*B*) UVRAG deficiency impairs C-Vps interaction with Q-SNAREs. 293T cells were transfected with control shRNA or UVRAG shRNA. WCLs were used for IP with anti-Vps16 (*Upper*) or anti-Vps18 (*Lower*), followed by IB with the indicated antibodies. (*Right*) Endogenous protein expressions are shown.

UVRAG Enhances C-Vps Interaction with SNAREs and *trans*-SNARE Assembly. The dual interactions of UVRAG with C-Vps and SNAREs through distinct domains (Fig. S7*G*) suggest that UVRAG may coordinate the complex assembly of C-Vps and SNAREs. More Vps16 or Vps18 coimmunoprecipitated with the Q-SNAREs when UVRAG was ectopically expressed (Fig. S7*D*). By contrast, deletion of the C2 or CCD, which abrogates C-Vps or Q-SNARE binding of UVRAG, respectively, failed to promote the C-Vps–SNARE interactions (Fig. S7*D*). In accord, knockdown of UVRAG severely hindered endogenous interaction of the C-Vps proteins with the SNAREs (Fig. 4*B*). These data indicate that UVRAG mediates the interaction of C-Vps with Q-SNAREs and may participate in the SNARE-mediated membrane fusion.

To investigate further whether UVRAG is also required in the assembly of cognate SNAREs into core complexes (Qa-Qb-Qc-R), a decisive step in driving membrane fusion (5, 24), we evaluated the *cis*- and *trans*-SNARE pairing in WT and UVRAG-depleted cells. Knockdown of UVRAG clearly reduced the interaction between Q-SNAREs without affecting their steady-level expression (Fig. S7*E*). Furthermore, the *trans*-SNARE assembly of the Q-SNARE with its cognate R-SNAREs VAMP8 and VAMP7 was also reduced when UVRAG was deficient (Fig. S7*E*). The marked effect of UVRAG on *trans*-SNAREs may influence their relative distribution at endosomal membranes. To explore this, we treated control and UVRAG-expressing HeLa cells with *N*-ethylmaleimide, which inhibits *N*-ethylmaleimide-sensitive fusion protein (NSF) and disassembly of SNARE complexes, and assessed the formation of the *trans*-SNARE complex by confocal microscopy. Both STX8 and the R-SNARE proteins VAMP7 and VAMP8 displayed punctate staining (Fig. S7*F*). Nearly complete colocalization was observed between the SNAREs in UVRAG-expressing cells, whereas only partial colocalization was detected in control cells (Fig. S7*F*). These results suggest that UVRAG promotes fusogenic SNARE complex formation during late endocytic membrane fusion in normal conditions.

VAMP8, but Not VAMP7, Is Required for Virus Entry. To determine the SNAREs involved in UVRAG-mediated virus entry, we depleted cells of individual SNAREs, including STX7, Vti1b,

MICROBIOLOGY

STX8, VAMP7, and VAMP8, and conducted one-step virus entry. As seen with inhibition of UVRAG, depletion of the Q-SNAREs or VAMP8 significantly blocked VSV-G–mediated virus entry (Fig. 5*A*). Intriguingly, no reduction was detected in VAMP7-deficient cells; instead, a slight increase resulted (Fig. 5*A*). As seen with VSV, suppression of VAMP8, but not VAMP7, rendered cells resistant to the pseudovirus infection of IAV, and it also drastically disabled the ability of UVRAG to promote virus entry, suggesting that UVRAG works in concert with specific SNAREs to regulate virus entry (Fig. S8 *A* and *B*). Given that UVRAG forms a complex with SNAREs through its CCD, these data explain the antiviral restriction of ΔCCD (Fig. 3*A*). Consistently, when cells were infected with live rVSV-GFP, only VAMP7 knockdown cells remained susceptible, whereas siRNA depletion of all other SNAREs was refractory to VSV infection (Fig. S8*C*). These results indicate that LE-associated Q-SNAREs and VAMP8 are specifically required for virus entry and infection.

Virus Entry Stimulates a Specific Complex Assembly of UVRAG, C-Vps, and SNAREs. The data above imply that UVRAG action with C-Vps and SNAREs is a key regulator during virus entry. This raises the question of whether this reflects a random event hitchhiked by the virus or, instead, a strategy of the virus to induce a specific fusogenic complex for efficient entry. To test this, we infected HeLa cells stably expressing empty vector or UVRAG with VSV and assessed the complex-forming ability of UVRAG with endogenous C-Vps and SNAREs within 2 h after infection (Fig. S8*D*). Compared with the complex formation in mock-infected cells, VSV infection triggered a robust increase of C-Vps and SNAREs coimmunoprecipitated with UVRAG (Fig. S8*D*). The increased binding was not due to differing expression because no evident alteration of the protein levels was detected in mock- and virus-infected cells (Fig. S8*D*). However, bafilomycin treatment significantly reduced the complex assembly of UVRAG with C-Vps and SNAREs (Fig. S8*D*), suggesting that this entry-induced complex assembly of UVRAG lies downstream of the low-pH trigger. As a control, the UVRAG–Beclin1 interaction was neither affected by VSV nor changed by bafilomycin (Fig. S8*D*), further suggesting that Beclin1 is not involved in this process. Analogous results were obtained when we infected cells with the pseudoparticles. As expected, VSV-G– and IAV-H5–mediated entry processes are sufficient to promote the complex formation of UVRAG, C-Vps, and Q-SNAREs (Fig. S8 *F* and *G*).

We next examined UVRAG-mediated *cis*- and *trans*-SNARE assembly upon viral infection. As shown in Fig. S8*E*, UVRAG expression enhanced interactions of STX7 with STX8 and Vti1b, as well as its pairing with VAMP8, which was further induced by VSV infection. In contrast, minimal amounts of VAMP7 coimmunoprecipitated with STX7, suggesting that VAMP7 is largely excluded from UVRAG-promoted SNARE complex formation upon viral infection (Fig. S8*E*). These findings demonstrate that virus entry triggers a specific supercomplex formation involving UVRAG, C-Vps, Q-SNARES, and VAMP8, but not VAMP7.

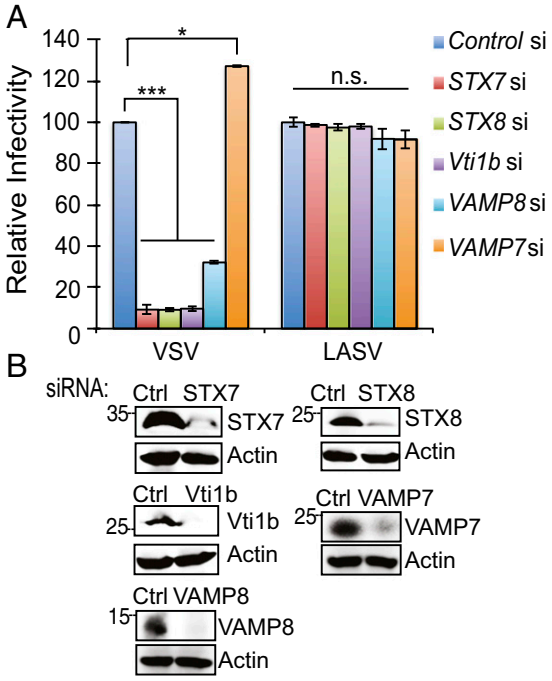

Fig. 5. Distinct roles of the SNARE proteins in virus entry. (*A* and *B*) HeLa cells were transfected with control- or SNARE-specific siRNA as indicated and then infected with pseudotyped viruses with the envelope protein of VSV and LASV for 48 h. (*A*) Viral entry is expressed as mean GFP fluorescence relative to control sh-treated cells. Values represent mean ± SD ($n = 3$ independent experiments). (*B*) Western blot shows endogenous protein expression in cells. n.s., not significant; $^*P < 0.05$; $^{***}P < 0.001$.

VAMP8 Recruitment to the Virus-Containing Vesicles. To examine whether VAMP7 and VAMP8 are differentially required for the virus entry-induced membrane remodeling, we examined endogenous redistribution of VAMP8 and VAMP7 in control and UVRAG-expressing cells after 1 h of infection with VSV (Fig. S9). Both VAMP8 and VAMP7 revealed vesicular staining with a perinuclear concentration in mock-infected cells (Fig. S9). Upon VSV infection, however, VAMP8 was prominently recruited to the VSV-G–containing vesicles, whereas VAMP7 was largely excluded (Fig. S9). Furthermore, expression of UVRAG resulted in a twofold increase in the acquisition of VAMP8-containing membranes to the VSV-G^+ vesicles compared with the control but had a minimal effect on VAMP7 accumulation in the virus-containing vesicles (Fig. S9). Although UVRAG is required for *trans*-SNARE complex assembly (Fig. S7*E*), only VAMP8 was selected to function with UVRAG in facilitating virus entry, whereas VAMP7 is largely absent from the majority of virus-containing compartments, consistent with an earlier finding that VAMP7 is not required for the entry of VSV and IAV.

Discussion

Initially discovered in a screen for UV resistance, UVRAG has been identified in our studies, as well as those of others, to possess various functions, including intracellular trafficking, chromosomal stability, autophagy activation, and tumor suppression (8–10, 12, 26, 27). However, the cellular outcome of UVRAG in viral infection has not been investigated. We show here that UVRAG-deficient cells are largely refractory to infection by VSV and the different types of IAV. Despite the fact that reduced autophagy makes a cellular milieu favorable for viral growth (14), suppression of UVRAG seems to override host autophagy machinery and to inhibit virus infection at a step upstream of viral replication. Indeed, the viral-resistant phenotype in UVRAG-depleted cells correlates with the impaired entry of VSV and IAV, both of which require acidic compartments to trigger their entry. We found that UVRAG operates late in the endocytic pathway by facilitating virus access to the LEs for membrane fusion in the cell. Furthermore, UVRAG regulation of viral entry requires C2 and CCD regions, which engage C-Vps and Beclin1, respectively (8, 9). Deletion of the C2 that disrupts the interaction with C-Vps tempered UVRAG-mediated viral entry. Unlike C-Vps, depletion of Beclin1 has a minimal effect on the action of UVRAG to promote viral infection, suggesting that other factors are involved in this process through the CCD. Indeed, UVRAG CCD is sufficient and necessary to bind LE Q-SNAREs in a manner independent of its association with C-Vps, serving as a regulator or a scaffold-like

protein in the assembly of the C-Vps–SNARE complex on the endosomes. Although C-Vps and SNAREs are central regulators of late endocytic organelles, their roles in modifying infection are less established. We demonstrated that abrogation of the subunit of C-Vps or Q-SNAREs drastically reduced entry processes of VSV and IAV. Unlike our findings, a recent study showed that C-Vps, albeit necessary for Ebola virus infection, is not needed in VSV infection (7). The discrepancy between published data and ours may be due to differences in experimental design and/or to the different cell lines used in the study. Nonetheless, our data suggests that for productive virus entry, both VSV and IAV cell entry must occur through the late endocytic pathway that is regulated by a functional UVRAG–C-Vps–Q-SNARE complex.

We found that a *trans*-SNARE complex consisting of the Q-SNAREs STX7, Vti1b, and STX8 and the R-SNARE VAMP8 is critical for virus entry and that the interaction of these SNAREs is enhanced shortly after VSV and IAV infection. In contrast, the Q-SNARE pairing with VAMP7 was drastically reduced. Previous studies have shown that VAMP7 is enriched on lysosomes, where it mediates heterotypic endosome–lysosome fusion, but that VAMP8 is present on LEs, where it controls homotypic fusion between these organelles (4). Conceivably, suppression of VAMP7, and thereby VAMP7-mediated lysosome fusion, may allow exclusion of endocytosed virions from the lysosome delivery designed for pathogen destruction and antigen presentation, whereas VAMP8 is needed for virus-induced membrane remodeling. In support of this, we found that VAMP8 is recruited to the virus-carrying vesicles, whereas VAMP7 is excluded. Moreover, unlike VAMP8, the depletion of which decreased virus entry, the knockdown of VAMP7 led to a slight but consistent increase of viral entry. Although further validation to elucidate the impact of SNAREs during in vivo infection is warranted, it is tempting to speculate that discrepant binding and SNARE assembly induced by viral infection could potentially reflect a strategy of the virus to evade lysosome degradation and immune recognition.

In summary, our study has identified a previously unknown function of UVRAG in the regulation of virus entry through multiple interactions with the membrane fusion machinery of cells, independent of IFN and autophagy activation. We have defined SNAREs required for endocytic transport and fusion of the virus, which, to our knowledge, has not been directly linked to virus entry before. Finally, the recruitment of specific cognate SNARE partners onto the target membrane reflects a virus-induced, highly programmed cascade of membrane fusion. Further understanding of the mechanism by which this cascade is regulated will have implications not only for the understanding of pathogenic mechanisms of virus entry but for development of attractive new targets for antiviral therapy.

Materials and Methods

MLV-GFP Pseudotyped Virus Preparation and Entry Assay. Pseudotyped MLV-GFP bearing different viral entry proteins was generated as described (18, 19). The entry proteins include IAV HA proteins from A/PR/8/34 [H1N1; H1(PR)], A/Udorn/72 [H3N2; H3(Ud)], and A/Thailand/2(SP-33)/2004(H5N1) [H5(Thai)], as well as glycoproteins from VSV, LASV, and LCMV. At 48 h postinfection with pseudotyped viruses, the cells were subjected to fluorescence microscopy and flow cytometry analysis to determine the GFP^+ cell population as previously described. Additional details of cell culture, virus purification and infection, plasmid constructs, confocal microscopy, flow cytometry, immunoprecipitation assay, and quantitative RT-PCR can be found in *SI Materials and Methods*.

Statistical Analysis. All experiments were independently repeated at least three times. Data are presented as mean ± SD. Statistical significance was calculated using the Student *t* test or one-way ANOVA test, unless otherwise stated. A P value of ≤ 0.05 was considered statistically significant.

ACKNOWLEDGMENTS. We thank the members of the C.L. laboratory for helpful discussion and Drs. S. P. Whelan, N. Mizushima, and J. Jung for providing reagents. This work is supported by American Cancer Society Grant RSG-11-121-01-CCG (to C.L.) and National Institutes of Health Grants R01 CA140964 and R21 CA161436 (to C.L.).

1. Gruenberg J (2009) Viruses and endosome membrane dynamics. *Curr Opin Cell Biol* 21(4):582–588.
2. Le Blanc I, et al. (2005) Endosome-to-cytosol transport of viral nucleocapsids. *Nat Cell Biol* 7(7):653–664.
3. Jahn R, Scheller RH (2006) SNAREs—Engines for membrane fusion. *Nat Rev Mol Cell Biol* 7(9):631–643.
4. Pryor PR, et al. (2004) Combinatorial SNARE complexes with VAMP7 or VAMP8 define different late endocytic fusion events. *EMBO Rep* 5(6):590–595.
5. Sato TK, Rehling P, Peterson MR, Emr SD (2000) Class C Vps protein complex regulates vacuolar SNARE pairing and is required for vesicle docking/fusion. *Mol Cell* 6(3):661–671.
6. Peterson MR, Emr SD (2001) The class C Vps complex functions at multiple stages of the vacuolar transport pathway. *Traffic* 2(7):476–486.
7. Carette JE, et al. (2011) Ebola virus entry requires the cholesterol transporter Niemann-Pick C1. *Nature* 477(7364):340–343.
8. Liang C, et al. (2008) Beclin1-binding UVRAG targets the class C Vps complex to coordinate autophagosome maturation and endocytic trafficking. *Nat Cell Biol* 10(7):776–787.
9. Liang C, et al. (2006) Autophagic and tumour suppressor activity of a novel Beclin1-binding protein UVRAG. *Nat Cell Biol* 8(7):688–699.
10. Takahashi Y, et al. (2007) Bif-1 interacts with Beclin 1 through UVRAG and regulates autophagy and tumorigenesis. *Nat Cell Biol* 9(10):1142–1151.
11. Zhao Z, et al. (2012) A dual role for UVRAG in maintaining chromosomal stability independent of autophagy. *Dev Cell* 22(5):1001–1016.
12. He S, et al. (2013) PtdIns(3)P-bound UVRAG coordinates Golgi-ER retrograde and Atg9 transport by differential interactions with the ER tether and the beclin 1 complex. *Nat Cell Biol* 15(10):1206–1219.
13. Katze MG, He Y, Gale M, Jr. (2002) Viruses and interferon: A fight for supremacy. *Nat Rev Immunol* 2(9):675–687.
14. Orvedahl A, Levine B (2009) Autophagy in Mammalian antiviral immunity. *Curr Top Microbiol Immunol* 335:267–285.
15. Shelly S, Lukinova N, Bambina S, Berman A, Cherry S (2009) Autophagy is an essential component of Drosophila immunity against vesicular stomatitis virus. *Immunity* 30(4):588–598.
16. Helenius A, Kartenbeck J, Simons K, Fries E (1980) On the entry of Semliki forest virus into BHK-21 cells. *J Cell Biol* 84(2):404–420.
17. Huang IC, et al. (2011) Distinct patterns of IFITM-mediated restriction of filoviruses, SARS coronavirus, and influenza A virus. *PLoS Pathog* 7(1):e1001258.
18. Brass AL, et al. (2009) The IFITM proteins mediate cellular resistance to influenza A H1N1 virus, West Nile virus, and dengue virus. *Cell* 139(7):1243–1254.
19. Rojek JM, Sanchez AB, Nguyen NT, de la Torre JC, Kunz S (2008) Different mechanisms of cell entry by human-pathogenic Old World and New World arenaviruses. *J Virol* 82(15):7677–7687.
20. Sieczkarski SB, Whittaker GR (2003) Differential requirements of Rab5 and Rab7 for endocytosis of influenza and other enveloped viruses. *Traffic* 4(5):333–343.
21. Lakadamyali M, Rust MJ, Babcock HP, Zhuang X (2003) Visualizing infection of individual influenza viruses. *Proc Natl Acad Sci USA* 100(16):9280–9285.
22. Kobayashi T, et al. (1999) Late endosomal membranes rich in lysobisphosphatidic acid regulate cholesterol transport. *Nat Cell Biol* 1(2):113–118.
23. Roth SL, Whittaker GR (2011) Promotion of vesicular stomatitis virus fusion by the endosome-specific phospholipid bis(monoacylglycero)phosphate (BMP). *FEBS Lett* 585(6):865–869.
24. Krämer L, Ungermann C (2011) HOPS drives vacuole fusion by binding the vacuolar SNARE complex and the Vam7 PX domain via two distinct sites. *Mol Biol Cell* 22(14):2601–2611.
25. Mercer J, Schelhaas M, Helenius A (2010) Virus entry by endocytosis. *Annu Rev Biochem* 79:803–833.
26. Liang C, Feng P, Ku B, Oh BH, Jung JU (2007) UVRAG: A new player in autophagy and tumor cell growth. *Autophagy* 3(1):69–71.
27. Liang C, Sir D, Lee S, Ou JH, Jung JU (2008) Beyond autophagy: The role of UVRAG in membrane trafficking. *Autophagy* 4(6):817–820.